Molecular docking, SAR analysis and biophysical approaches in the study of the antibacterial activity of ceramides isolated from Cissus incisa

Deyani Nocedo-Mena, Sonia Arrasate, Elvira Garza-González, Verónica M. Rivas-Galindo, Antonio Romo-Mancillas, Cristian R. Munteanu, Nuria Sotomayor, Esther Lete, Iratxe Barbolla, César A. Martín, María del Rayo Camacho-Corona,

Bioorganic Chemistry, Volume 109, 2021, 104745

https://doi.org/10.1016/j.bioorg.2021.104745

Highlights

- Isolated ceramides **(1)** from *Cissus incisa* leaves are new within genus
- Ceramides **(1)** were more active against carbapenems-resistant *Acinetobacter baumannii*
- Molecular docking showed that ceramides **(1)** target on Gram-negative cell membrane
- Biophysical assay shown that **(1)** disturb membrane permeability without lithic action
- The set of obtained results allow enunciate a preliminary mechanism of action

Graphical Abstract

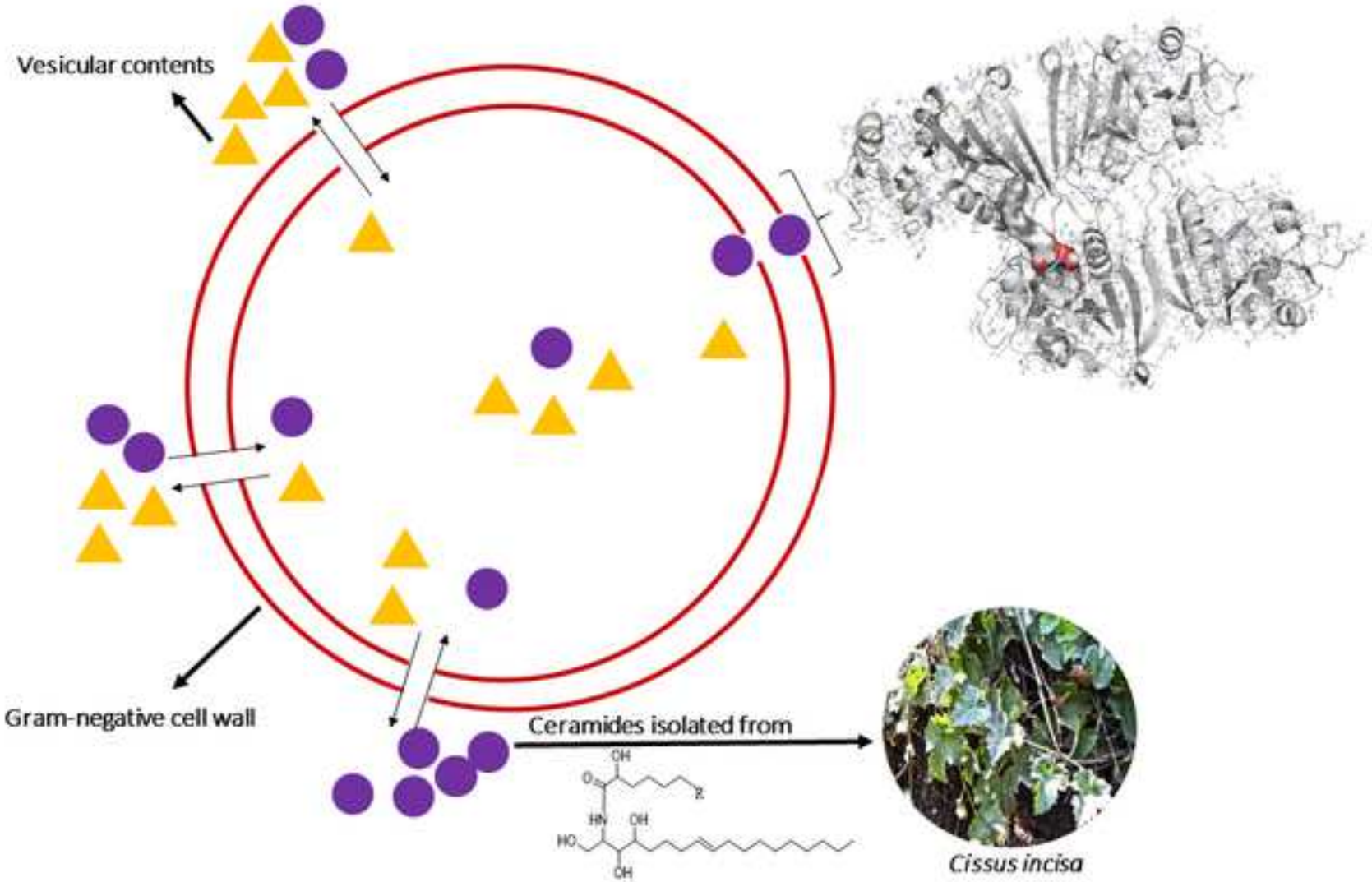

Molecular docking, SAR analysis and biophysical approaches in the study of the antibacterial activity of ceramides isolated from *Cissus incisa*

Deyani Nocedo-Mena[a,b], Sonia Arrasate[b], Elvira Garza-González[c], Verónica M. Rivas-Galindo[d], Antonio Romo-Mancillas[e], Cristian R. Munteanu[f,g,h], Nuria Sotomayor[b], Esther Lete[b], Iratxe Barbolla[b], César A. Martín[*i,j], María del Rayo Camacho-Corona[a*]

[a]Universidad Autónoma de Nuevo León, Facultad de Ciencias Químicas. Av. Universidad S/N, Ciudad Universitaria, 66451, San Nicolás de los Garza, Nuevo León, México.

[b]University of the Basque Country UPV/EHU, Department of Organic Chemistry II, 48940, Leioa, Spain.

[c]Universidad Autónoma de Nuevo León, Servicio de Gastroenterología, Hospital Universitario "Dr. José Eleuterio González". Av. Gonzalitos and Madero S/N, Colonia Mitras Centro, 64460, Monterrey, Nuevo León, México.

[d]Universidad Autónoma de Nuevo León, Facultad de Medicina. Av. Gonzalitos and Madero S/N, Colonia Mitras Centro, 64460, Monterrey, Nuevo León, México.

[e]Universidad Autónoma de Querétaro, Facultad de Ciencias Químicas, Centro Universitario, Cerro de las Campanas, 76010, Querétaro, México.

[f]University of A Coruna, Computer Science Faculty, 15071 A Coruña, Spain.

[g] Instituto de Investigación Biomédica de A Coruña (INIBIC), Complexo Hospitalario Universitario de A Coruña (CHUAC), 15006 A Coruña, Spain.

[h]Centro de Investigación en Tecnologías de la Información y las Comunicaciones (CITIC), Campus de Elviña s/n 15071 A Coruña, Spain

[i]Biofisika Center, CSIC UPV/EHU, 48940, Leioa, Spain.

[j]University of the Basque Country, UPV/EHU, Department of Biochemistry and Molecular Biology, Faculty of Science and Technology, 48940, Leioa, Spain.

Corresponding authors:

[*a] Email: maria.camachocn@uanl.edu.mx. Tel:+52(81)8329-4000(3414)

[*i,j] Email: cesar.martin@ehu.eus .Tel: 0034946018052

ABSTRACT

The developing of antibacterial resistance is becoming in crisis. In this sense, natural products play a fundamental role in the discovery of antibacterial agents with diverse mechanisms of action. Phytochemical investigation of *Cissus incisa* leaves led to isolation and characterization of the ceramides mixture (**1**): (8*E*)-2-(tritriacont-9-enoyl amino)-1,3,4-octadecanetriol-8-ene **(1-I)**; (8*E*)-2-(2´,3´-dihydroxyoctacosanoyl amino)-1,3,4-octadecanetriol-8-ene **(1-II)**; (8*E*)-2-(2´-hydroxyheptacosanoyl amino)-1,3,4-octadecanetriol-8-ene **(1-III)**; and (8*E*)-2-(-2´-hydroxynonacosanoyl amino)-1,3,4-octadecanetriol-8-ene **(1-IV)**. Until now, this is the first report of the ceramides **(1-I)**, **(1-II)**, and **(1-III)**. The structures were elucidated using NMR and mass spectrometry analyses. Antibacterial activity of ceramides **(1)** and acetylated derivates **(2)** was evaluated against nine multidrug-resistant bacteria by Microdilution method. **(1)** showed the best results against Gram-negatives, mainly against carbapenems-resistant *Acinetobacter baumannii* with MIC=50 μg/mL. Structure-activity analysis and molecular docking revealed interactions between plant ceramides with membrane proteins, and enzymes associated with biological membranes of Gram-negative bacteria, through hydrogen bonding of functional groups. Vesicular contents release assay showed the capacity of **(1)** to disturb membrane permeability detected by an increase of fluorescence probe over time. The membrane disruption is not caused for ceramides lytic action on cell membranes, according *in vitro* hemolytic activity results. Combining SAR analysis, bioinformatics and biophysical techniques, and also experimental tests, it was possible to explain the antibacterial action of these natural ceramides.

Keywords: *Cissus incisa*; *Acinetobacter baumannii*; molecular docking; vesicular contents assay; hemolysis.

1. Introduction

The developing of antibacterial resistance is becoming a burden to clinicians, researchers, and the population in general. The evolution and widespread distribution of antibiotic-resistance elements in bacterial pathogens have made diseases that were once easily treatable, today be deadly [1]. The World Health Organization (WHO) proposed a global priority pathogen list of Multi-Drug Resistant (MDR) bacteria to guide research, discovery, and development of new antibiotics. Carbapenems-resistant (CR) *Acinetobacter baumannii*, CR *Klebsiella pneumoniae*, and MDR *Pseudomonas aeruginosa* are most serious ESKAPE organisms, considered among major cause of hospital-acquired infections [2]. The emergence of MDR Gram-negative bacilli creates a challenge in the treatment of nosocomial infections. These bacteria have an additional membrane layer that serves as a barrier, disabling of most antibacterial compounds to go through it and reach their intended target. Therefore, the development of compounds that target the outer membrane barrier and improve the influx of antibiotics could be successful in treating these resistant bacteria. Using combinatorial therapy may be the key to overcoming antibacterial resistance, associating a membrane permeabilising agent with an antibacterial with a different mechanism of action [3], [4].

Unfortunately, accompanying the rise on global resistance is a failure in novel antibacterial drug discovery. In this sense, natural products became a special interest. Natural products have historically been of crucial importance in the identification and development of antibacterial agents. Many phytochemical investigations are under way to identify novel chemical skeletons with antibacterial activity. Recently, has been reported chemo-informatics approaches for the identification of potential natural antibiotics and their mechanism of action [5]. Among them, molecular docking has a very important role in the rational design of drugs. This technique allows predicting the affinity and activity of a drug candidate molecule with the protein where it will act. Otherwise, different systems of membrane models are used for the study of lipid and protein interactions. Among them, liposomes have been the most widely used system to study basic biophysical and biochemical phenomena related to cell membranes [6]. Large Unilamellar Vesicles (LUV) are the type of liposomes most used as model membranes. They have unique characteristics that make them the most suitable for studying the possible interactions of compounds with cell membranes [7].

As a part of the scientific authentication to the Mexican flora, our research group carried out the phytochemical research of *Cissus incisa*. This plant is endemic from North

Mexico and the southern part of the United States; belonging to Vitaceae family. According to traditional Mexican medicine, leaves are used to treat infectious diseases like respiratory and skin infections, as well as abscesses [8]. Previously we reported phytol, *β*-amyrin, cerebrosides, *α*-amyrin, *β*-sitosterol and its respective glycosides, and the antibacterial activity of chloroform/methanol extract from *C. incisa* leaves [8,9] [10]. Further research in the $CHCl_3$/MeOH extract led to isolation and structural elucidation of ceramides mixture **(1),** and then their acetylated derivatives **(2)** were obtained. Their structures were elucidated using spectroscopic and spectrometric data. To our knowledge, ceramides **1-I**, **1-II** and **1-IV** had not been reported before. Natural ceramides **(1)** showed antibacterial activity on CR *A. baumannii*. Several approaches were used to enunciate their mode of action. Structure-activity analysis (SAR) was in agreement with molecular docking studies. Ceramides **(1)** produced the release of the fluorescent probe by modifications on membrane permeability through pores formation and not due to a lytic action of membranes. This was evidenced by the vesicular contents assay of LUV and the hemolysis test.

2. Material and methods

2.1 General

Column chromatography used as stationary phase: silica gel (SiO_2) brand EMD chemicals Inc. with a particle size 0.040-0.063 mm. Mobile phases were hexane, chloroform, ethyl acetate from Sigma-Aldrich (St. Louis, Missouri, USA), MeOH grade Baker reactive and dichloromethane reagent grade brand Macron Chemicals. Thin-Layer Chromatography (TLC) silica gel 60 F254 20 x 20 cm plates, Merck KGA. Spectroline brand UV lamp (λ=254nm and 365nm) and ceric sulfate solution in sulfuric acid were used as developers. Nuclear Magnetic Resonance (NMR) spectra were obtained from a Bruker-400 spectrometer operated at 400 MHz (^1H) and 100 MHz (^{13}C) with tetramethylsilane as internal standard. UltraHigh Performance Liquid Chromatography (UHPLC) was carried out using an ACQUITY UPLC™ system from Waters (Milford, MA, USA), equipped with binary solvent delivery pump, autosampler, and column oven. A reverse-phase column (Acquity UPLC C18 CSH, 100 × 2.1 mm, 1.7 μm) and pre-column (Acquity UPLC C18 CSH 1.7 μm VanGuardTM) were used at 65 °C. All MS data were acquired on SYNAPT G2 HDMS, with a quadrupole time of flight (Q-ToF) analyzer (Waters, Milford, MA, USA) equipped with an electrospray ionization (ESI) source that operated in positive mode.

2.2 Phytochemical study

C. incisa leaves were collected in Rayones, locality belongs to Nuevo Leon, Mexico (Latitude: 25.0167°, Longitude: -100.05°, Altitude: 900 m). The collection was made in October 2016. A reference sample was deposited in the herbarium of the Faculty of Biology of the Autonomous University of Nuevo Leon with the voucher 027499.

The plant material was drying at room temperature and grinding to obtain 809 g of grounded material. This was extracted by maceration with $CHCl_3$/MeOH (1:1) for 48 h. It was performed filtration and then *in vacuum* distillation of organic extract seven times until was obtained 84 g of dried extract. Then, it was fractionated by CC using silica gel (1680g) with gradients of Hex/EtOAc/MeOH, yielding 403 fractions. Fractions were analyzed by TLC and pooled according to their chromatographic similarity obtaining 24 pooled fractions (fr. A to X). Fr. S (EtOAc 100 %) and U (EtOAc/MeOH 80:20) were joined (3.685 g) because of chromatographic similarity and then analyzed by CC with DCM/MeOH gradients until obtained 114 sub-fractions. Sub-fraction 60-62 (DCM/MeOH 89:11; 23.5 mg) was washed several times with Hex and acetone yielding 21.8 mg (0.0027%) of a yellow solid **(1)**.

Ceramides **(1)**, mp 139-141°C. HRMS-ESI (positive-ion mode) *m/z*: 790 $[M+H]^+$, 753 $[M]^+$, 723 $[M]^+$, and 751 $[M]^+$. UHPLC-QToF-MS *m/z*: 789.5898 $[M]^+$ ($C_{51}H_{99}NO_4$, calc. 789.7574); 753.5657 $[M]^+$ ($C_{46}H_{91}NO_6$, calc. 753.6846); 723.6073 $[M]^+$ ($C_{45}H_{89}NO_5$, calc. 723.6741); 751.6426 $[M]^+$ ($C_{47}H_{93}NO_5$, calc. 751.7054. ^1H and ^{13}C NMR data in Table 1.

2.3 Acetylation of **(1)**

Acetylation reaction proceeded in the same way to previous studies [9], with acetic anhydride (0.7 mL) and pyridine (0.3 mL). It was obtained the acetylated derivate **(2)** as a white solid (9.0 mg, 88.7%).

Acetylated ceramides **(2)**, mp 55-57°C. $C_{57}H_{105}NO_7$ (calc. 915.79 g/mol); $C_{56}H_{101}NO_{11}$ (calc. 963.74 g/mol); $C_{53}H_{97}NO_9$ (calc. 891.72 g/mol); $C_{55}H_{101}NO_9$ (calc. 919.75 g/mol), ^1H and ^{13}C NMR data, see Table 1.

Table 1. NMR ^{1}H (400 MHz) and ^{13}C (100 MHz) data of **(1)** and **(2)**

Position	**(1)** ($CDCl_3$/MeOD)		**(2)** ($CDCl_3$)	
	^{1}H	^{13}C	^{1}H	^{13}C
1	3.78 m	61.35	1α-4.36 (dd, *J* (Hz) =11.72, 6.36) 1β-4.03 (dd, *J* (Hz) =11.64, 3.14)	62.41
2	4.12 m	51.94	4.46 m	47.84
3	3.54 m	75.71	5.12 m	74.03
4	3.54 m	72.26	4.97 m	72.73
5	1.42 m	32.92	1.65 m	28.57
6	1.42 m	26.19	1.34 brs	24.91
7	1.98 m	32.92	1.99 m	32.61
8	5.41 m	131.01	5.42 m	131.19
9	5.41 m	130.21	5.36 m	129.29
10	1.69 m	33.07	1.99 m	32.21
$(CH_2)_n$	1.27 brs	25.49-32.23	1.25 brs	25.53-31.80
CH_2-CH_3	1.27 brs	22.96	1.25 brs	22.71
Me	0.88 m	14.21	0.90 (t, *J* =6.66 Hz)	14.13
NH	7.59 (d, *J*=6.32 Hz)	-	6.65 (d, *J*=9.08 Hz)	-
1´	-	176.22	-	170.00
2´	4.04 m	72.62	5.12 m	72.25
3´	3´α-1.78 m 3´β-1.58 m	34.78	1.84 m	31.94
CH_3CO-1	-	-	2.05 s	20.70
CH_3CO-3	-	-	2.11 s	20.88
CH_3CO-4	-	-	2.08 s	20.77
CH_3CO-2´	-	-	2.20 s	21.03
CH_3CO-1	-	-	-	170.05
CH_3CO-3	-	-	-	170.95
CH_3CO-4	-	-	-	170.02
CH_3CO-2´	-	-	-	171.31

2.4 Antibacterial activity

Double-distilled water, dimethyl sulfoxide (DMSO) (JT Baker, USA), INC-80 incubator (Prendo), sterile 96-well round-bottom microplates with lid (Corning Costar, New York), and Mueller Hinton medium were used (Becton Dickinson). Nine strains of drug-resistant clinical isolates were obtained from University Hospital Dr. Eleuterio González of the Autonomous University of Nuevo Leon. Four of these bacteria are included in the list of priority pathogens issued by the WHO [2].

Gram-positive bacteria: Methicillin -Resistant *Staphylococcus aureus* (14-2095), Linezolid-resistant *Staphylococcus epidermidis* (14-583), Vancomycin - resistant *Enterococcus faecium* (10-984). Gram-negative bacteria: CR *A. baumannii* (12–666), *Escherichia coli* producing Extended-Spectrum Beta-Lactamase (14-2081), *P. aeruginosa* resistant to carbapenems (13-1391), CR *Klebsiella*

pneumoniae NDM-1+ (14-3335), *K. pneumoniae* producer of ESBL (14-2081) and CR *K. pneumoniae* (OXA-48 positive).

Microdilution method was used to determine the antibacterial activity of **(1)** and **(2)**, following the methodology described in [11]. The range of concentrations used was: 200, 100, 50, 25, 12.5, 6.25, and 3.12 μg/mL. Levofloxacin was used as positive control with the same concentrations, and DMSO (6% to 0.09%, v/v) was used as negative control. All the experiments were conducted in triplicates. The MIC was determined as the Minimum Concentration of the compound that inhibits the growth of the bacteria.

2.5 Molecular Docking

The strength of the interactions was quantified by the Affinity Energy (AE) of ligands to the protein targets using the open software AutoDockVina [12]. This *target fishing* procedure, focused in targets of representative bacteria, was done into the BioCAI cluster from the University of A Coruna (Spain). The docking flow has several steps that include the ligand and protein processing, conversion and geometry optimization before the docking calculations. Thus, ligands were presented as a list of SMILES formula and they were converted into PDB with the optimized 3D structure using Babel software [13]. The protein targets were filtered for only the first PDB model; the non-protein part was eliminated (water molecules, other ligands, *etc*.). The PDB of ligands and proteins were converted into PDBQT format using AutoDock Tools scripts (prepare_ligand4.py and prepare_receptor4.py) [14]. The protein target was considered rigid in all docking calculations and the interaction searching was considering the entire surface of the targets. The docking flow was based on python and bash scripts, including the reading of the final results. The cut-off for stable interactions was considered AE < -7.0 kcal/mol [15]. The study was based on a screening of **(1)** and **(2)** against Gram-negative bacteria as they were the most sensitive in the experimental study. However, results were based on the first docking conformer of the ligands with a reference root-mean-square deviation of atomic positions (RMSD) of 0 [16].

2.6 Release of vesicular contents assay

The assay was developed at Biofisika Institute (UPV/EHU, CSIC), following the protocol developed by Hope *et al* [17]. 1,2-Di-oleoyl-*sn*-glycero-3-phosphocholine (DOPC) Large Unilamelar Liposomes (LUV) were prepared. Determination of phospholipid concentration in the LUV preparations was carried out by the colorimetric method describe by Fiske and Subbarow [18].

2.6.1 Vesicular contents release assay

The method used to perform this assay was described by Ellens *et al* [19]. It is based on the attenuation of the ANTS fluorescence by the DPX. Both molecules were encapsulated in the interior of the liposomes, so the DPX attenuates the fluorescence of the ANTS by their close distance. The release of the contents of the LUV to the outside environment as a consequence of the rupture of the permeability barrier of the bilayer leads to an increment of the fluorescence emitted by ANTS as the distance of the DPX in the medium does not allow an efficient quenching.

The assays for the release of the vesicular contents were performed in a Fluoromax-3 fluorometer taking measurements at fixed wavelengths, an excitation maximum at 355 nm and emission at the 520 nm of the ANTS. The grid opening for both monochromators was set at 5 nm and a 475 nm filter was used in the emission monochromatic to reduce the signal due to excitation light scattering. In the kinetics the change in the initial signal of the liposomes was followed after the addition of the compound, approximately 300 min. To finish the reaction and obtain the maximum fluorescence of the ANTS, Triton X-100 was added at a concentration that completely solubilized the vesicles. Then, the fluorescence value corresponding to 100% of release was obtained. The percentage of release caused by **(1)** was quantified using the following equation (i):

$$\% \text{ Release} = \frac{(F_f - F_0)}{(F_{100} - F_0)} \times 100 \qquad \text{(i)}$$

F_f=fluorescence after the addition of **(1)**; F_0=initial value of the fluorescence of the vesicles; F_{100} =fluorescence after the solubilization of the liposomes by the Triton X-100.

2.7 Hemolytic activity assay

Hemolytic assay was carried out using the protocol described by Bellalou *et al* [20]. The technique involved the incubation of ram erythrocytes (Pronadisa, Spain) with serial dilutions of **(1)**. The lysis of the erythrocytes was determined by quantifying the hemoglobin released into the medium, after 4h of incubation using a spectrophotometer. To calculate the percentage of hemolysis of the samples, the equation (ii) was used:

$$\% \text{ Hemolysis} = \frac{(\text{Abs}_{412\text{ nm sample}} - \text{Abs}_{412\text{ nm }0\%})}{\text{Abs}_{412\text{ nm }100\%}} \times 100 \qquad \text{(ii)}$$

3. Results and discussion

3.1 Structural characterization of **(1)** and **(2)**

Ceramides **(1)** were analyzed by UHPLC-QToF-MS. Chromatogram of **(1)** revealed a succession of four abundant peaks at different t_R indicating the presence of a mixture of homologous compounds (Figure 1). The abundance percentages observed on the chromatogram were: 21.33 % (**1-I**, t_R 1.61 min); 47.40 % (**1-II**, t_R 4.20 min); 13.27 % (**1-III**, t_R 9.66 min); and 18.0 % (**1-IV**, t_R 12.45 min); being **1-II** the most abundant. HRMS-ESI spectra (positive mode) of each peak showed molecular ions at *m/z* 790 $[M+H]^+$ (**1-I**), 753 $[M]^+$(**1-II**), 723 $[M]^+$ (**1-III**), and 751 $[M]^+$ (**1-IV**).

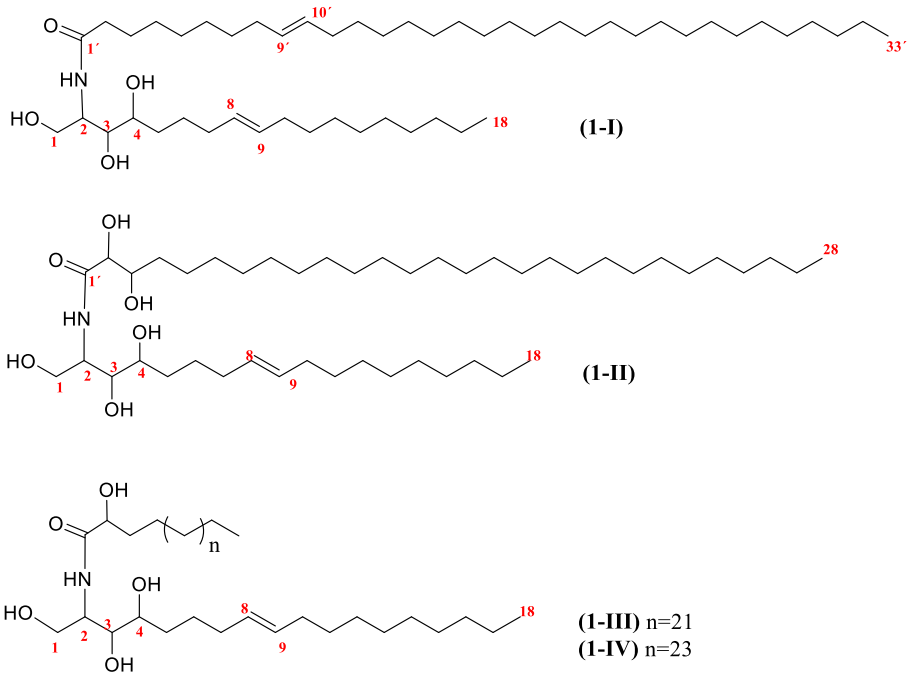

Figure 1. Chemical structures of **(1)**

A secondary amide group was deduced analyzing the ^1H and ^{13}C NMR spectra by the following signals: nitrogen attached proton at δ_H 7.59 (d, J =6.32 Hz), a nitrogen-attached carbon at δ_C 51.94 and carbonyl group at δ_C 176.22. The ^1H NMR also showed signals of terminal methyls (δ_H 0.88, m; δ_C 14.21), multiple proton signals between δ_H 1.42-1.98 (m, δ_C 32.92-33.07) and broad singlet (δ_H 1.27, δ_C 22.96-32.23) characteristics of two long-aliphatic chains that confirmed the presence of a ceramide.

Ceramides constitutes the hydrophobic backbone of all complex sphingolipids, and structurally consists of a Long Chain Base (LCB) attached at an amide bond to a fatty

acid with a variable length chain. Most plant LCB_s have eighteen carbons, although small amounts of other chain lengths have also been reported. Very Long Chain Fatty Acid (VLCFA) can also undergo modifications, which lead to at a variety of sphingolipid isoforms in plants [21].

HSQC spectra revealed four hydroxylated carbons at δ_C 61.35 (C1), 75.71 (C3), 72.26 (C4) and 72.62 (C2'). Meanwhile COSY spectra showed important correlations between the positions of the LCB: H-2/H-1 (δ_H 4.12/δ_H 3.78); H-2/H-3 (δ_H 4.12/δ_H 3.54); and NH proton (δ_H 7.59) with H-2 (δ_H 4.12) (Figure 2). The complete structure of **(1)** was established using 1D and 2D NMR data combined with HRMS-ESI.

Olefinic protons at δ_H 5.41 (H-8 and H-9) were attributable to double bond, supported by two ethylenic carbons at δ_C 131.0 (C8) and δ_C 130.21 (C9). Double bond was determined to be *trans* according to the chemical shifts of the allyl carbons δ_C 32.92 (C-7) and δ_C 33.07 (C-10) [25]. Double bond was localized on position C8-C9 of the LCB by biogenetic considerations [22]. The confirmation was found in the HRMS-ESI spectra by the fragments *m/z* 153 $[C_{11}H_{21}]^+$ and *m/z* 127 $[C_9H_{19}]^+$ resulting from the rupture of the LCB on both sides of the double bond (Figure 3), in addition to the correlations COSY among the vinyl hydrogens H-8/H-9 (δ_H 5.41), with H-7 (δ_H 1.98) (Figure 2).

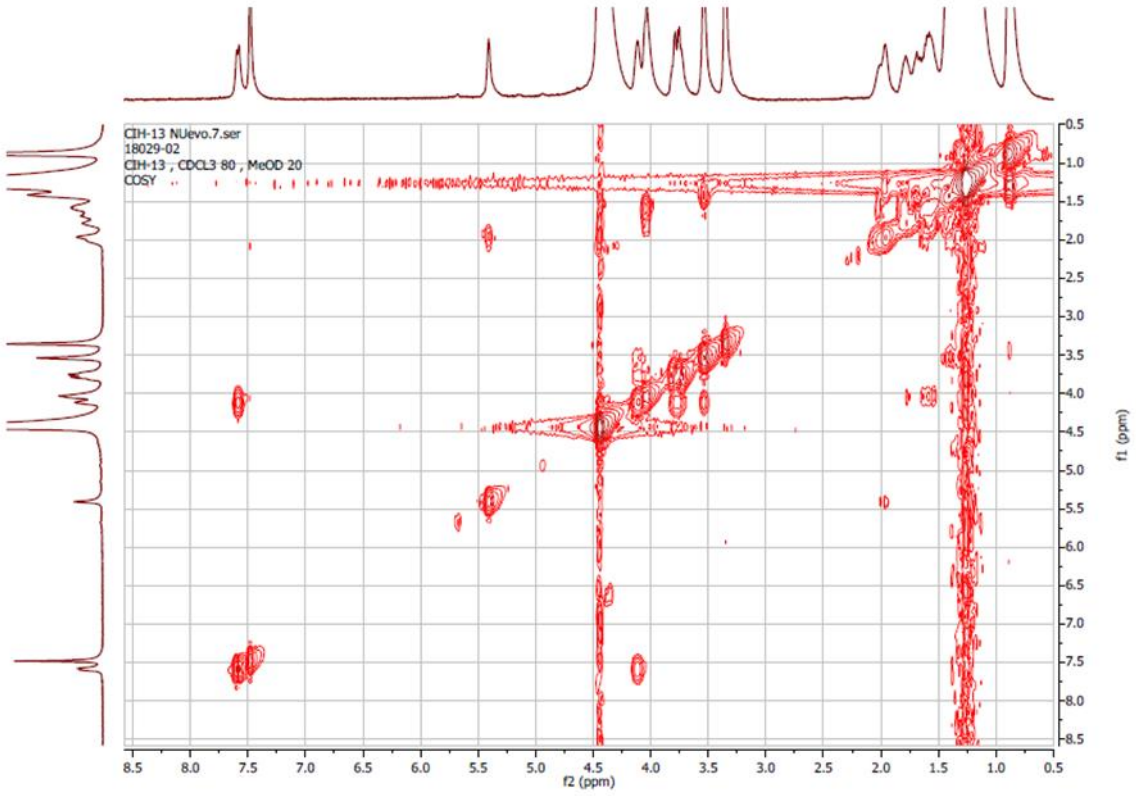

Figure 2. COSY of **(1)**

A 1,3,4 trihydroxylated LCB was determined by a typical rupture in ceramides (α to carbonyl) to obtain the *m/z* 342, confirming the 18C trihydroxylated LCB (Figure 3), in agreement with other researchers [22].

The length of the α-hydroxylated fatty acid chains was determined in the same way that Wang *et al*. [23] using the ion peaks observed in the HRMS-ESI. In the case of ceramide **1-I** the ion of the complete VLCFA (tritriacont-9-enoic acid) was not observed. Instead, some fragments that justified this fatty acid were observed at: *m/z* 323 $[C_{23}H_{47}]^+$, 153 $[(C_{10}H_{16}O)+1]^+$, 167 $[C_{10}H_{17}NO]^+$ which correspond to ruptures α to double bond, α to carbonyl and to nitrogen, respectively (Figure 3). For ceramides **1-II** and **1-III**, both fatty acids (2,3-dihydroxyoctacosanoic acid; 2-hydroxyheptacosanoic acid) and LCB_s were confirmed by the presence of its base peaks (BP) *m/z* 663 $[C_{46}H_{81}NO]^+$ and *m/z* 684 $[C_{45}H_{82}NO_3]^+$ respectively, formed in both cases due to the loss of water molecules (Figure 3). For ceramide **1-IV**, the VLCFA was checked by *m/z* 406 $[C_{28}H_{54}O]^+$ corresponding to ruptures α to carbonyl of 2-hydroxynonacosanoic acid (Figure 3). There are reported ceramides with several fatty acid modifications where α-hydroxylation (position 2´) as the most common. However, other ceramides with hydroxylation at C-2´and C-3´, were also previously informed [24]. Other modifications described for the fatty acyl components of ceramides are the absence of hydroxylation, variable length, and desaturation in the ω-9 position [22].

These results coincide with those studies about plants sphingolipids, particularly ceramides, relating to main modifications of the LCB_s in plants: hydroxylation in C4 and unsaturation Δ8. The latter is absent in mammals and fungi, but very common in plants and yeasts. In the same way, agreements are manifested for the variations in the fatty acid chains described above and those of the literature [22].

Finally, the spectroscopic data were compared with the data of previous characterized ceramides [26] finding similarities that confirm **(1)** is a ceramide. Based on the earlier discussion, **(1)** was determined as a mixture of (8*E*)-2-(tritriacont-9-enoyl amino)-1,3,4-octadecanetriol-8-ene (**1-I**); (8*E*)-2-(2´,3´-dihydroxyoctacosanoyl amino)-1,3,4-octadecanetriol-8-ene (**1-II**); (8*E*)-2-(2´-hydroxyheptacosanoyl amino)-1,3,4-octadecanetriol-8-ene (**1-III**); (8*E*)-2-(2´-hydroxynonacosanoyl amino)-1,3,4-octadecanetriol-8-ene (**1-IV**). As far we know, this is the first report of ceramides **1-I**, **1-II** and **1-IV** in the literature. Furthermore, is the first characterization of all ceramides within the genus *Cissus*. HRMS-ESI spectra, 1D and 2D NMR spectra of **(1)** can be consulted in Supplementary data.

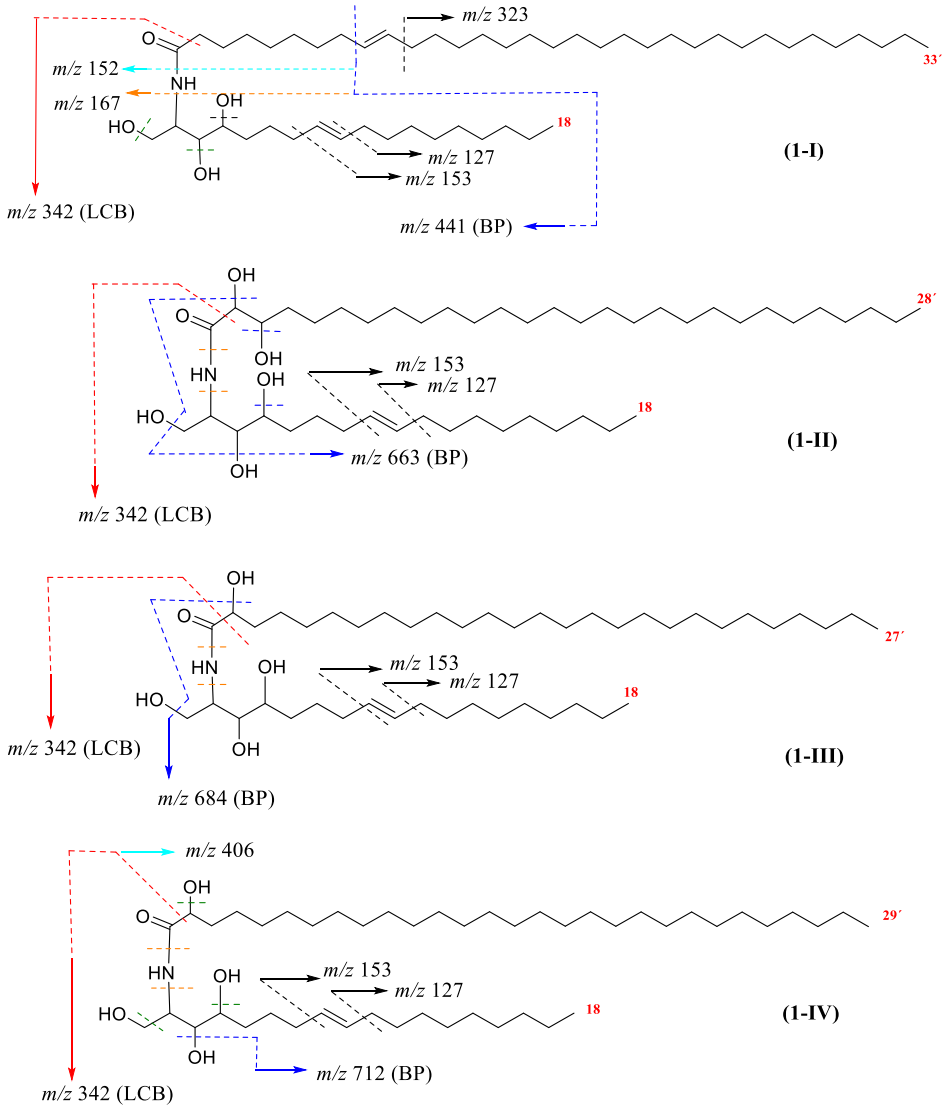

BP: Base peak; LCB

Figure 3. Fragmentation patterns of **(1)** that justify ions obtained in the HRMS-ESI spectra

Acetylation of **(1)** yielded the acetylated derivate **(2)**, which was analyzed by ^{1}H and ^{13}C NMR. The 1D and 2D NMR spectra showed the spectroscopic data that confirmed the main structure of ceramides.

The acetylated derivative **(2)** also presented the signals of double bond at δ_H 5.36 (H-9) and δ_H 5.42 (H-8), which was located at position 8 of the LCB responding to biogenetic origin [22] and supported by COSY correlation between protons H-7/H-8 (δ_H 1.99/δ_H 5.42) (Figure 4). The double bond was determined to be *trans*, according to the chemical shifts of neighboring carbons [25]. The ceramides skeleton was assigned using the HSQC experiment, observing the direct correlations of protons with their respective carbons and comparing with the spectroscopic data of a similar derivative obtained from

the roots of *Gynura japonica* by Lin *et al* [27]. The presence of a 1,3,4-triacetylated LCB was deduced from the ^{1}H-^{1}H COSY data. Thus, the signal at δ_H 6.65 (N-H), gave a cross peak with the signal at δ_H 4.46 (H-2) which, in turn, showed crossed peaks with methylene protons (H-1, δ_H 4.36 and δ_H 4.03) and with H-3 (δ_H 5.12). The latter was correlated with the signal at δ_H 4.97 (H-4) (Figure 4).

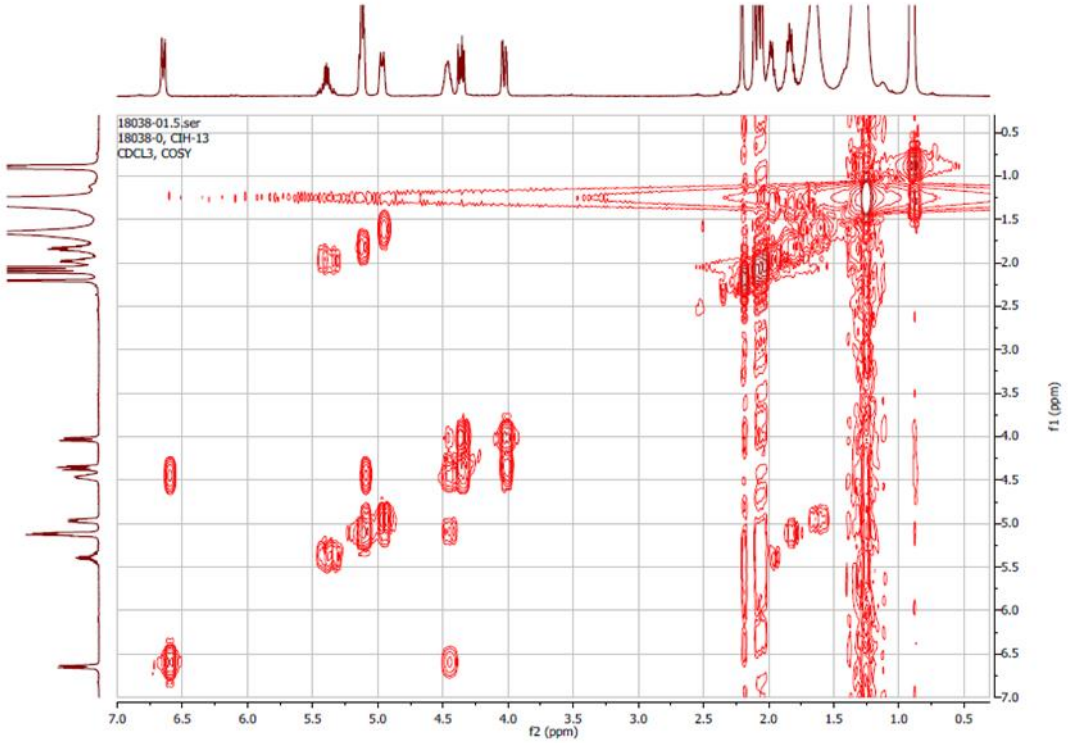

Figure 4. COSY of **(2)**

^{1}H NMR of acetylated derivative **(2)** showed four singlets of acetyl groups in δ_H (ppm): 2.05 (CH_3CO-1), 2.08 (CH_3CO-4), 2.11 (CH_3CO-3), 2.20 (CH_3CO-2´). ^{13}C NMR spectra showed four methyl groups of acetyl groups localized at δ_C (ppm): 20.70 ($\underline{CH_3}CO$-1), 20.77 ($\underline{CH_3}CO$-4), 20.88 ($\underline{CH_3}CO$-3), 21.03 ($\underline{CH_3}CO$-2´), and their respective carbonyl groups in δ_C (ppm): 170.02 ($CH_3\underline{CO}$-4), 170.05 ($CH_3\underline{CO}$-1), 170.95 ($CH_3\underline{CO}$-3), 171.31 ($CH_3\underline{CO}$-2´). Based on the above, **(2)** was determined as a mixture of: (8*E*)-2-(tritriacont-9-enoyl amino)-1,3,4-octadecanetriacetat-8-ene (**2-I**); (8*E*)-2-(2´,3´-diacetoxyoctacosanoyl amino)-1,3,4-octadecanetriacetat-8-ene (**2-II**); (8*E*)-2-(2´-acetoxyheptacosanoyl amino)-1,3,4-octadecanetriacetat-8-ene (**2-III**); and (8*E*)-2-(2´-acetoxynonacosanoyl amino)-1,3,4- octadecanetriacetat-8-ene (**2-IV**) (Figure 5). Until our best knowledge, these derivatives have no reports in the literature. 1D and 2D NMR spectra of **(2)** can be consulted in Supplementary data.

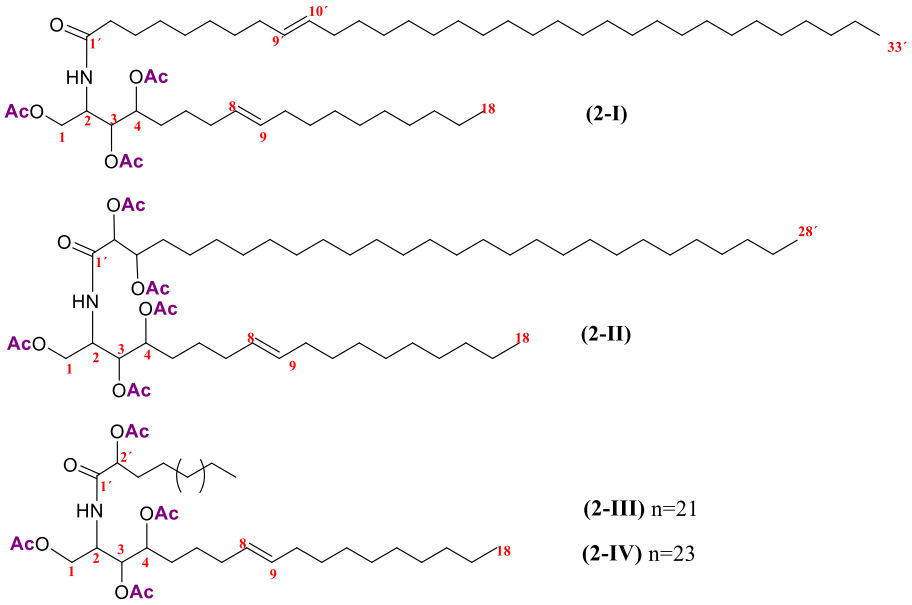

Figure 5. Chemical structures of **(2)**

3.2 Antibacterial activity

Results of antibacterial activity of **(1)** and **(2)** against clinical isolates of MDR bacteria are shown in Table 2. The best result was reached by **(1)** against the Gram-negative bacteria with MIC values of 50-200 µg/mL. This result is extremely important since these dangerous pathogens have an incredible ability to develop antimicrobial resistance. The most sensitive strain was CR *A. baumannii* with MIC=50 µg/mL. The effect of **(1)** against *A. baumannii*, is remarkable and interesting. *A. baumannii* has a number of resistance mechanisms, including β-lactamases, aminoglycoside-modifying enzymes, efflux pumps, permeability defects, and modifications of target sites. Therefore, several strains of *A. baumannii* are highly resistant to most of the clinically available antibiotics [28].

To obtain semi-synthetic derivatives is a strategy used to improve multiple characteristics of natural antibiotics such as: potency and spectrum, particularly activity against resistant organisms [29]. Nevertheless, in this work, the semi-synthetic derivative **(2)** did not exceed those of its natural product **(1)**. Excepting for vancomycin-resistant *E. faecium*, where **(2)** showed the best activity (MIC=100 µg/mL), even better than **(1)**. Maybe this result was obtained because of the structural differences of the thick peptidoglycan layer formed by abundant lipids in Gram-positives.

Table 2. Antibacterial activity of **(1)** and **(2)** (MIC µg/mL)

Strains	**1**	**2**	**levofloxacin**
Methicillin-resistant *S. aureus*	>200	>200	12.5
Linezolid-resistant *S. epidermidis*	>200	>200	6.25
Vancomycin-resistant *E. faecium*	200	100	12.5
Carbapenems-resistant *A. baumannii*	**50**	200	12.5
E. coli producing ESBL	>200	>200	25
P. aeruginosa resistant to carbapenems	100	200	0.78
Carbapenems-resistant *K. pneumoniae* (NDM-1+)	200	>200	>50
K. pneumoniae producer of ESBL	200	>200	12.5
Carbapenems-resistant *K. pneumoniae* (OXA-48 positive)	200	200	>50

(1): natural ceramides; **(2)**: acetylated ceramides

3.3 Structure-activity analysis

Recently plants sphingolipids had not been widely studied. New plant lipid structures are still being identified, and different approaches are being used to help understanding their full potential. In this context, this work seeks the link between the experimental results and the evaluated ceramides.

Ceramides, like all sphingolipids, form hydrogen bonding, groups such as O-H and N-H can act as hydrogen bond donors and acceptors. These groups are responsible for proper orientation of ceramide in a bilayer membrane and are involved in the formation of an interfacial hydrogen-bonding network typical of sphingolipids [30]. In addition, these groups are also responsible for the ceramide fulfilling its biological function, because these groups bind to the active sites of membrane proteins.

Comparing the antibacterial activity of **(1)** *vs* **(2)**, practically the acetyl derivate **(2)** had no action. The lack of the OH group, specifically in position 1 could explain the low activity observed for **(2)**. Mouts *et al*. [30] demonstrated that complete removal of the primary alcohol dramatically reduced the ability of ceramide to form ceramide-rich ordered domains, giving special importance to functional groups C-1(OH) of the LCB. According with their own results, C-3(OH) does not appear equally important for ceramide's co-lipid interactions.

Our experimental findings are consistent with previous studies, showing the ceramides requirements to display their biological activities. Ceramides depend of the polar groups (specially in C-1) to develop their action thought hydrogen binding.

3.4 Molecular docking

Molecular docking is one of the most frequently used methods in structure-based drug design, due to its ability to predict the binding-conformation of ligands to the target binding site. The *target fishing* procedure was performed only for targets identified as relevant for Gram-negative pathogens since those species were the most sensitive in experimental study. Only the conformations with a docking score below -7.0 kcal/mol [15] were considered the most favorable binding conformations and worthy of further analysis. On this basis, remarkable ligand-protein interactions were obtained for the pathogens' molecular targets tested and the results were based on the best scored conformer.

The best macromolecular targets identified were a mutant of *E. coli* lipoprotein embedded between the outer membrane and the periplasmic peptidoglycan (PDB 1t8z) [31], *K. pneumoniae* dihydrofolate reductase (PDB 4osg) [32], hemophore HasAp of *P. aeruginosa* (PDB 3mom) [33], and *A. baumannii* outer membrane channel DcaP (PDB 6eus) [34].

Figures 6-9, show docking images for the best protein-ligand complex for each pathogen, as well as ligand interaction diagram (LID) of the protein-ligand complex (calculated using ProteinsPlus [35] web server). The best interaction obtained was for the complex ceramide and *E. coli* lipoprotein, with AE = -9.3 kcal/mol. This result was expected due to the highly lipophilic nature of the target and the ligand. The ceramide showed lower affinity to the rest of the biological targets. Less stable interactions were obtained for *A. baumannii* membrane channel and *K. pneumoniae* dihydrofolate reductase, both with AE= -7.6 kcal/mol. (See Supplementary data for a complete list of targets).

Molecular docking studies showed possible interactions with proteins located in the cell membranes of Gram-negative bacteria, as well as oxidoreductase proteins, membrane proteins, transport proteins, and signaling in different cellular processes. By analyzing the ceramide structural requirements with molecular docking results, it is highlighted the importance of the polar groups of ceramide in its antibacterial activity. From the above, we approach the presentation of a preliminary mechanism of action for ceramides, with the cell membrane as the target. The membrane is an attractive and underexploited target of antimicrobials. In this sense, it has been informed a natural product (violacein) against Gram-positive pathogens targeting the cytoplasmic membrane [36].

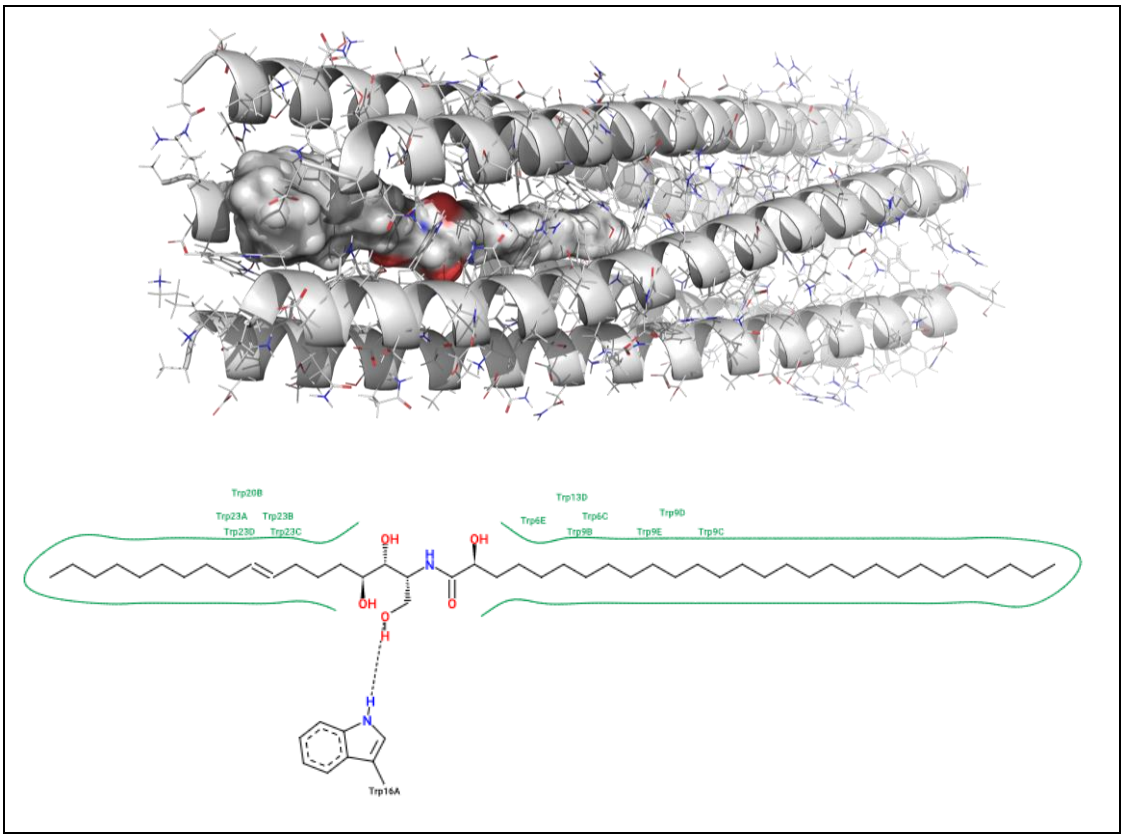

Figure 6. Best complex **1-II**/*E. coli* target (PDB 1t8z, AE = -9.3 kcal/mol). Hydrophobic regions are highlighted in green. In blue and red, hydrophilic regions.

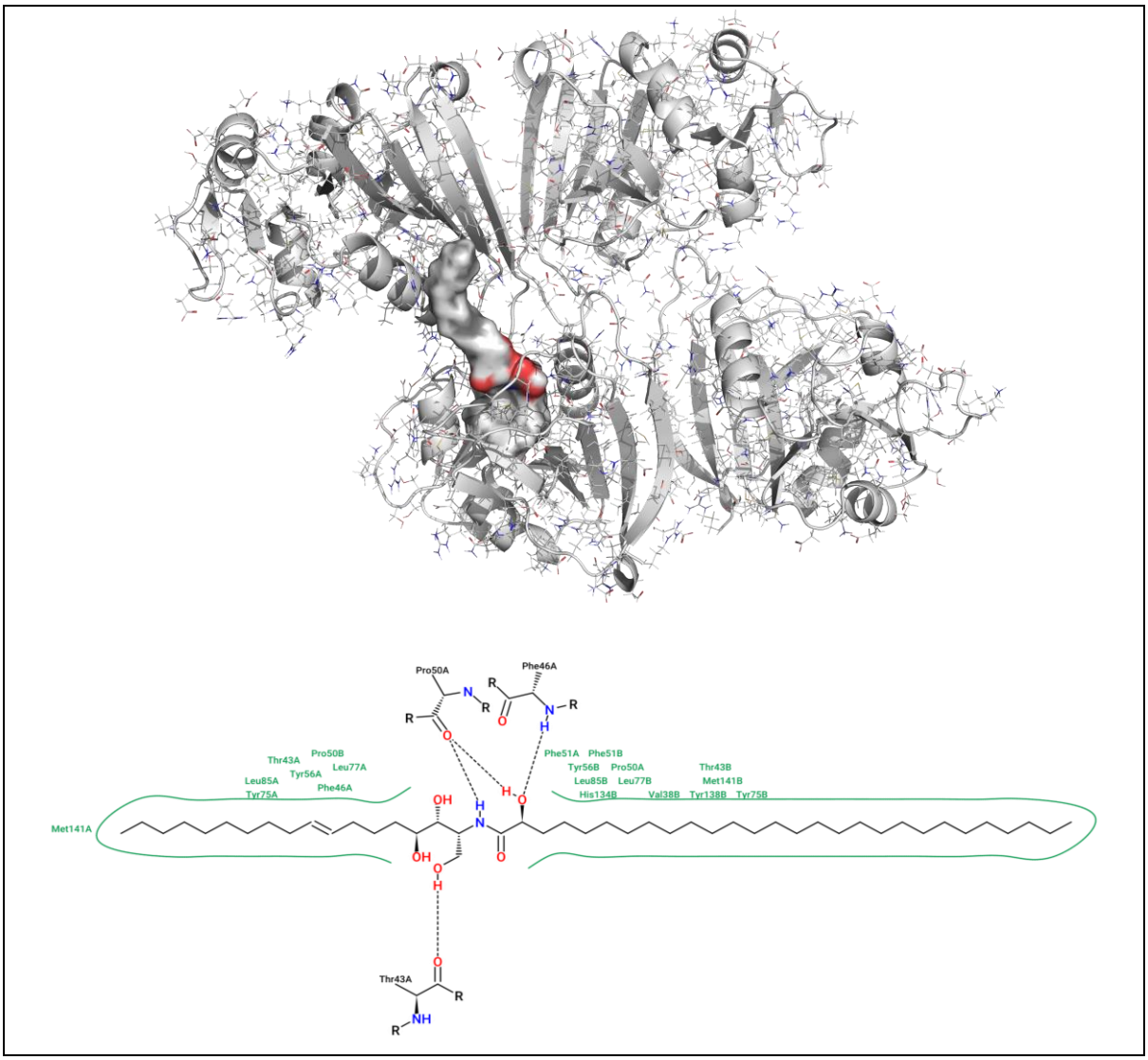

Figure 7. Best complex **1-II**/*K. pneumoniae* target (PDB 4osg, AE = -7.6 kcal/mol). Hydrophobic regions are highlighted in green. In blue and red, hydrophilic regions.

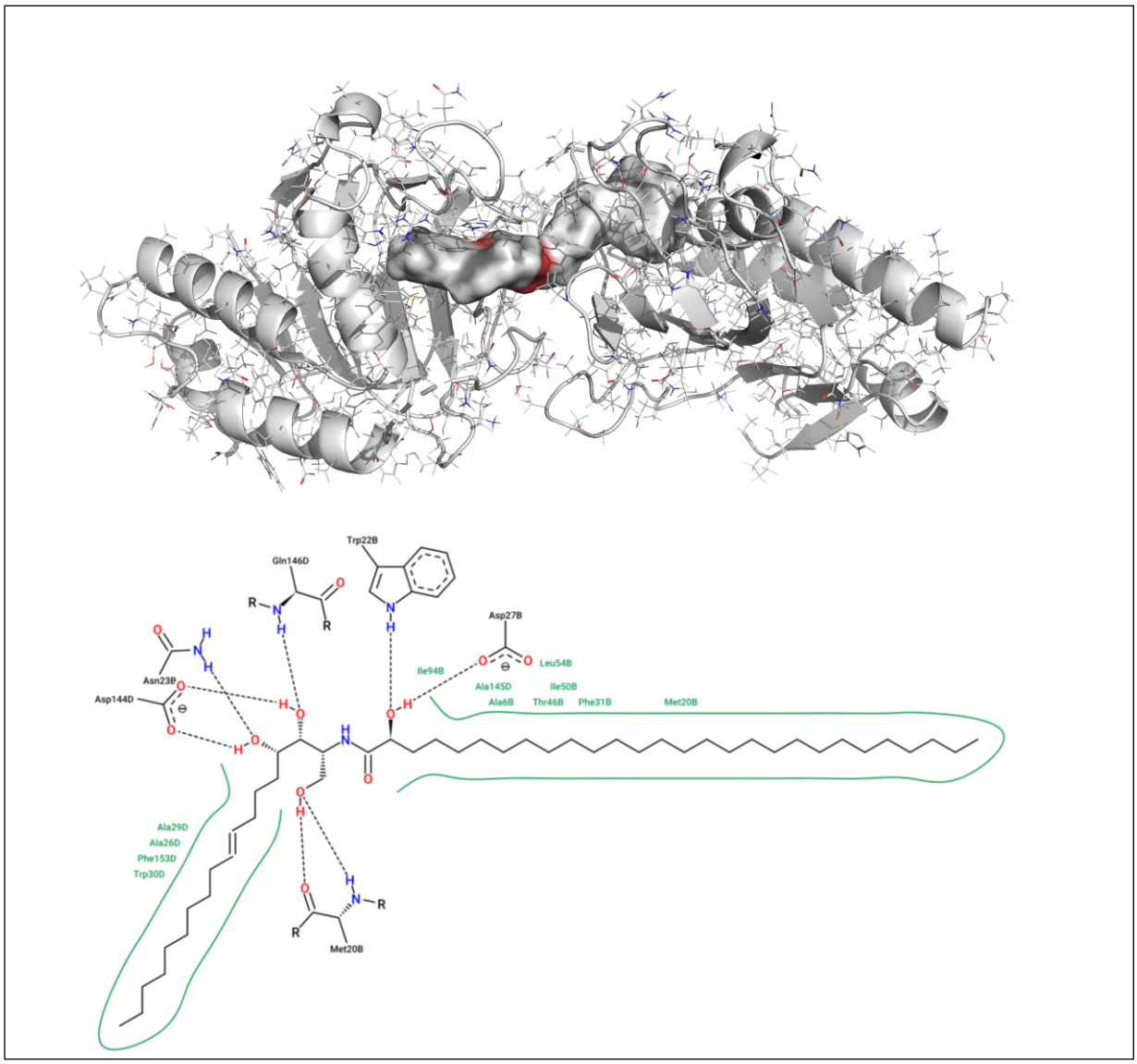

Figure 8. Best complex **1-II**/*P. aeruginosa* target (PDB 3mom, AE = -8.1 kcal/mol). Hydrophobic regions are highlighted in green. In blue and red, hydrophilic regions.

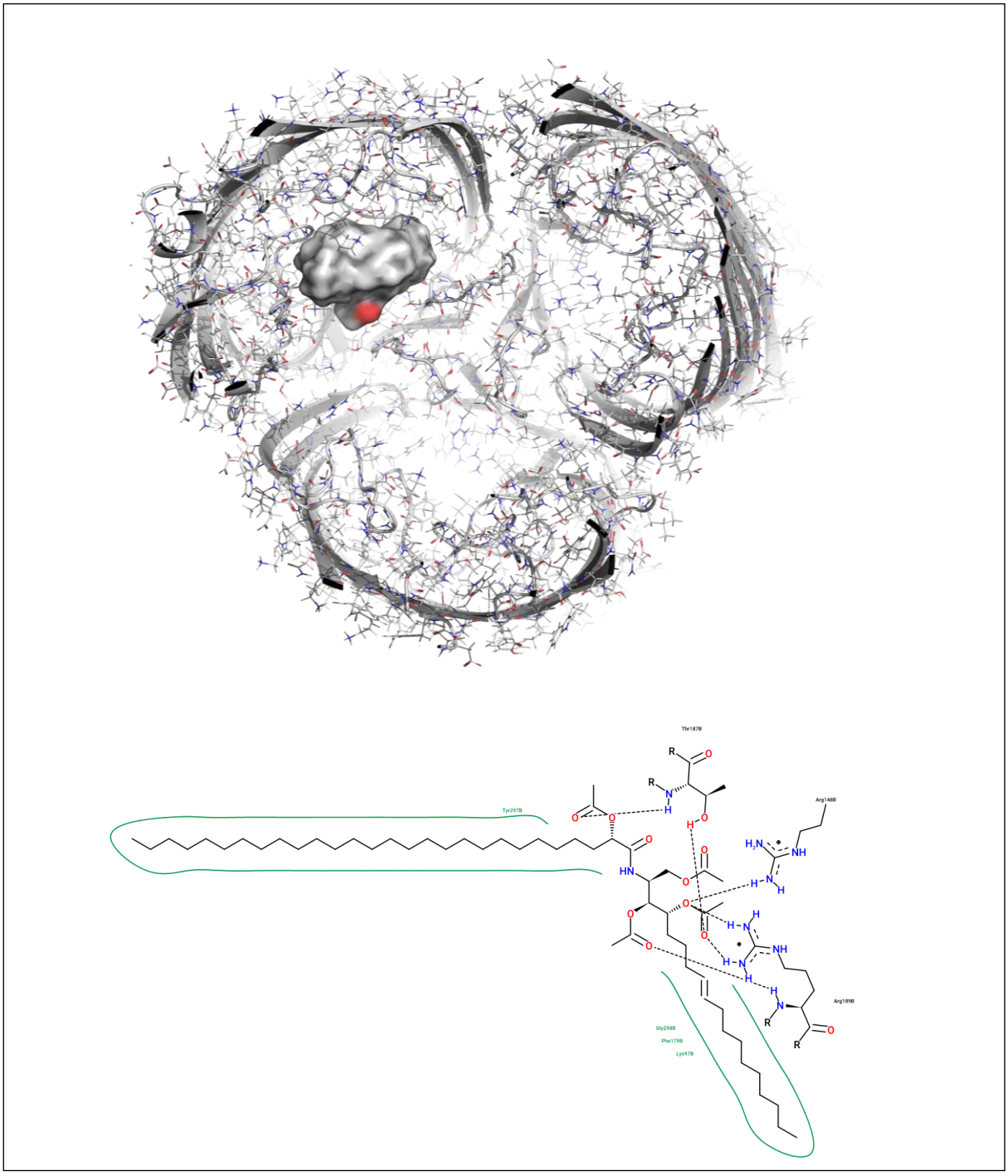

Figure 9. Best complex **2-II**/ *A. baumannii* target (PDB 6eus, AE = -7.6 kcal/mol). Hydrophobic regions are highlighted in green. In blue and red, hydrophilic regions.

3.5 Vesicular contents release assay

The effect of **(1)** on the cell membrane was determined using a contents release assay with the ANTS fluorescent probe. Figure 10 shows an increase in the fluorescence of the probe over time. This phenomenon is consequence of the effect of the **(1)** on LUV permeability. Ceramides perturb membrane permeability, which was detected by the efflux of ANTS. The release of vesicular contents caused by ceramides was slow,

increasing gradually with the time. No release was observed in the first 90 minutes after ceramides were added. Furthermore, Figure 11 shows the best result at the highest concentration (13.6 μM) used in the experiment.

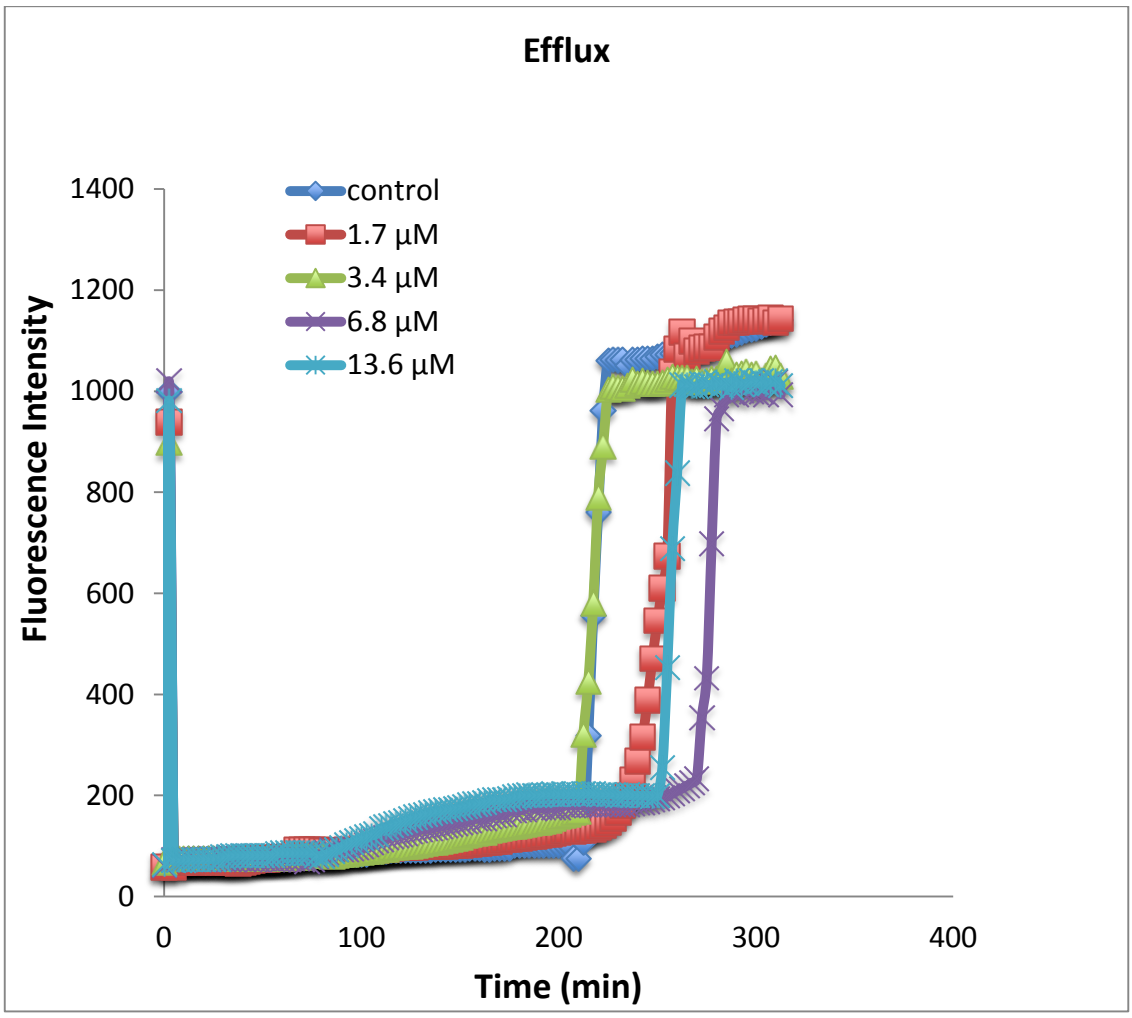

Figure 10. Efflux of ANTS-DPX induced by the action of **(1)**

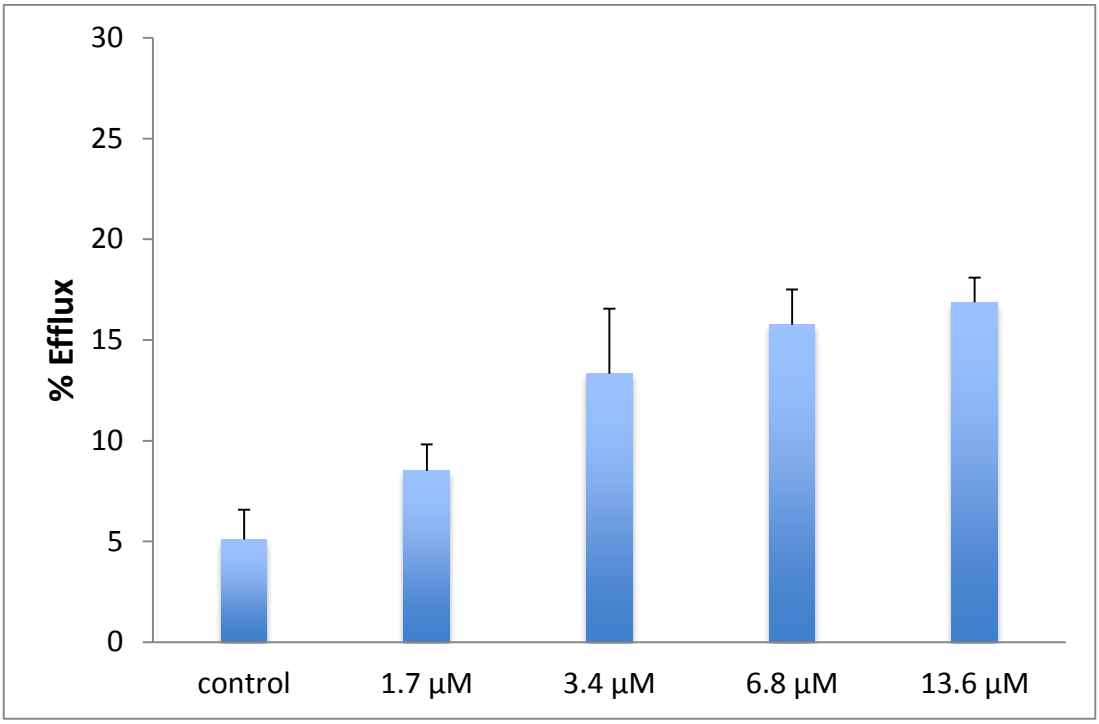

Figure 11. Ceramides **(1)** induced concentration-dependent efflux of solutes encapsulated in LUV

The capacity of synthetic ceramides to modify the permeability barrier of cell membranes has been previously explored [37]. The finding that ceramides **(1)** have antibacterial properties directed to the cell membrane should lay the groundwork for future research on the usefulness of this natural product. Considering the destabilization on cell membrane permeability, it is possible to propose a combination with an antibacterial agent with different mechanism of action. It has been reported that co-encapsulation of a molecule with antitumor activity and the ceramide results in an increase in the activity of the first [38]. Moreover, the combination ceramide-antibacterial drug against resistant bacteria could reverse multidrug-resistance; even the antibacterial MIC could be reduced.

3.6 Hemolytic activity assay

In vitro hemolysis study is often used as a sensitive and reliable method to assay the lytic action on cell membranes of any physical or chemical agent. Ceramides **(1)** did not cause hemolysis to the ram erythrocytes tested. This result was in agreement with those reported for other *Cissus* species. Several studies have exposed that species within this genus are safe for humans and not toxic [39]. However, further experiments will need

to carry out in animal models, as this is currently the only way to assess the overall toxicity of any compound.

The fact that **(1)** exhibits slow release of vesicular contents, suggests that the permeability mechanism of LUV does not consist in solubilizing the membrane similar to a detergent. Ceramides cause transient holes and/or phase separation that allows the passage of molecules through the membrane, in agreement with the results of Artetxe *et al* [40].

The results obtained in this study allow to propose a possible mechanism of action for ceramides isolated from *C. incisa* leaves. Although the experimental result point out to *A. baumannii* as the most sensitive target, other features draw attention to the Gram-negative bacteria tested. Previous studies have suggested that the geometry of ceramide change cells membrane permeability [41]. In addition to these biophysical properties, they can interact with targets at the membrane level through hydrogen bonding, resulting in permeability disturb. Ceramides target the Gram-negative cell membrane, which can facilitate the entry of antibiotics into the bacteria. Ours findings opens the doors for future research that decides to address the problem of antibacterial shortages in a different way. Maybe the solution is not in discovering new drugs, but rather allows existing ones to act, facilitating them to go through into the bacterial cell.

Conclusions

This work reports the first characterization of ceramides **1-I, 1-II, 1-III** in the literature. Further, all ceramides here presented are reported within genus *Cissus* for first time. Ceramides **(1)** showed activity against Gram-negative bacteria. A combination of structure-activity analysis, bioinformatics and biophysical techniques made possible to explain the antibacterial action of these natural ceramides. The cell membrane destabilization caused by ceramides makes them interesting candidates for future studies in drug discovery from natural sources as well as adjuvant treatments. Ceramides from *C. incisa* could induce a synergistic antibacterial effect with current standard therapies and offer alternative solutions to overcome the antibiotic resistance, mainly to Gram-negatives.

Glossary

AE=Affinity Energy; Cer=Ceramide; CC=Column Chromatography; DCM=dichloromethane; EtOAc=ethyl acetate; ESBL=Extended Spectrum Beta-lactamases; ESI=Electrospray Ionization; fr= fraction; Hex=hexane; LCB=Long Chain Base; LUV=Large Unilamellar Vesicles; MeOH=methanol; MDR=Multi Drug

Resistant; MIC=Minimum Inhibitory Concentration; SAR=Structure-activity relationships; UHPLC=Ultrahigh Performance Liquid Chromatography

Acknowledgments

D.N.M, thanks financial support from CONACYT grant (No. 605522) and for Mobility Scholarships Abroad 2018 (291250). Results are taken in part from the PhD thesis of D.N.M. M.d.R.C.C. and D.N.M. acknowledges biologist M. González Ferrara, for plant identification and sample collection. As well as kind collaboration of the personnel of the UANL Hospital Gastroenterology Service Laboratory, and the Department General Services of UPV, Spain. Special thanks to Jone Amuategi for her participation in hemolysis tests. S.A., N.S., and E.L. acknowledge research grants from the Ministry of Economy and Competitiveness, MINECO, Spain (No. FEDER CTQ2016-74881-P), and the Basque government (No. IT1045-16). C.R.M. thanks to a) the Collaborative Project in Genomic Data Integration (CICLOGEN) PI17/01826 funded by the Carlos III Health Institute from the Spanish National plan for Scientific and Technical Research and Innovation 2013-2016 and the European Regional Development Funds (FEDER)-"A way to build Europe"; b) the Spanish Ministry of Economy and Competitiveness for its support through the funding of the unique installation BIOCAI (UNLC08-1E-002, UNLC13-13-3503) and the European Regional Development Funds (FEDER) by the European Union; c) the Consolidation and Structuring of Competitive Research Units - Competitive Reference Groups (ED431C 2018/49), funded by the Ministry of Education, University and Vocational Training of the Xunta de Galicia endowed with EU FEDER funds.

Formatting of funding sources

This research did not receive any specific grant from funding agencies in the public, commercial, or not-for-profit sectors.

Supplementary data

Supplementary data to this article can be found online at XXXX

AUTHORS INFORMATION

Corresponding authors

*E-mail: maria.camachocn@uanl.edu.mx (M.d.R.C.C.)

*E-mail: cesar.martin@ehu.eus (C.A.M)

ORCID

Deyani Nocedo Mena: 0000-0001-8061-8609

Sonia Arrasate: 0000-0003-2601-5959

[5] M. Arias, H. Vogel, Fluorescence and Absorbance Spectroscopy Methods to Study Membrane Perturbations by Antimicrobial Host Defense Peptides, in: P. Hansen (Ed.), Antimicrob. Pept. Methods Protoc. Methods Mol. Biol., Copenhague, 2017: pp. 141–157. https://doi.org/10.1007/978-1-4939-6737-7_10.

[6] Gómez Bilbao, G. Adenilato ciclasa de Bordetella pertussis estudio de su interacción con membranas. (Universidad del País Vasco - Euskal Herriko Unibertsitatea, 2009).

[7] M.A. Alvarado Vázquez, A. Rocha Estrada, S. Moreno Limón, De la lechuguilla a las biopelículas vegetales: las plantas útiles de Nuevo León, Monterrey, Nuevo León, México, 2010.

[8] D. Nocedo-Mena, C. Cornelio, M.D.R. Camacho-Corona, E. Garza-González, N. Waksman De Torres, S. Arrasate, N. Sotomayor, E. Lete, H. González-Díaz, Modeling Antibacterial Activity with Machine Learning and Fusion of Chemical Structure Information with Microorganism Metabolic Networks, J. Chem. Inf. Model. 59 (2019) 1109–1120. https://doi.org/10.1021/acs.jcim.9b00034.

[9] D. Nocedo-Mena, V.M. Rivas-Galindo, P. Navarro, E.G.- González, L. González-Maya, M.Y. Ríos, A. García, F.G. Ávalos-Alanís, J. Rodríguez-Rodríguez, M. del R. Camacho-Corona, Antibacterial and cytotoxic activities of new sphingolipids and other constituents isolated from *Cissus incisa* leaves., Heliyon. 6 (2020). https://doi.org/10.1016/j.heliyon.2020.e04671.

[10] D. Nocedo-Mena, E. Garza-González, M. González-Ferrara, M. Camacho-Corona, Antibacterial Activity of *Cissus incisa* Extracts against Multidrug-Resistant Bacteria, Curr. Top. Med. Chem. 20 (2020) 1–6. https://doi.org/10.2174/1568026619666191121123926.

[11] J.R. Zgoda, J.R. Porter, A Convenient Microdilution Method for Screening Natural Products Against Bacteria and Fungi, Pharm. Biol. 39 (2001) 221–225. https://doi.org/10.1076/phbi.39.3.221.5934.

[12] O. Trott, A.J. Olson, AutoDock Vina: improving the speed and accuracy of docking with a new scoring function, efficient optimization and multithreading, J Comput Chem. 31 (2011) 455–461. https://doi.org/10.1002/jcc.21334.

[13] N. O´Boyle, M. Banck, C.A. James, C. Morley, T. Vandermeersch, G.R. Hutchison, Open Babel: An open chemical toolbox, J. Cheminform. 3 (2011) 1–14. http://www.jcheminf.com/content/3/1/33.

[14] G.M. Morris, R. Huey, W. Lindstrom, M.F. Sanner, R.K. Belew, D.S. Goodsell, A.J. Olson, AutoDock4 and AutoDockTools4: Automated Docking with Selective Receptor Flexibility, J Comput Chem. 30 (2010) 2785–2791. https://doi.org/10.1002/jcc.21256.

[15] M.W. Chang, W. Lindstrom, A.J. Olson, R.K. Belew, Analysis of HIV Wild-Type and Mutant Structures via *in Silico* Docking against Diverse Ligand Libraries, J. Chem. Inf. Model. 47 (2007) 1258–1262.

[16] E.A. Coutsias, C. Seok, K. Dill, Using quaternions to calculate RMSD, J Comput Chem. 25 (2004) 1849–57. https://doi.org/10.1002/jcc.20110.

[17] M. Hope, M. Bally, G. Webb, P. Cullis, Production of large unilamellar vesicles by a rapid extrusion procedure: characterization of size distribution, trapped volume and ability to maintain a membrane potential, Biochim Biophys Acta. 812 (1985) 55–65.

[18] C.H. Fiske, Y. Subbarow, The colorimetric determination of phosphorus, J. Biol. Chem. 66 (1925) 375–400.

[19] H. Ellens, J. Bentz, F. Szoka, H+- and Ca2+-induced fusion and destabilization of liposomes, Biochemistry. 24 (1985) 3099–106.

[20] J. Bellalou, H. Sakamoto, D. Ladant, C. Geoffroy, A. Ullmann, Deletions affecting hemolytic and toxin activities of *Bordetella pertussis* adenylate cyclase, Infect Immun. 58 (1990) 3242–3247.

[21] D.D. V Lynch, T.M.T. Dunn, An introduction to plant sphingolipids and a review of recent advances in understanding their metabolism and function, New Phytol. 161 (2004) 677–702. https://doi.org/10.1111/j.1469-8137.2003.00992.x.

[22] L. V. Michaelson, J.A. Napier, D. Molino, J.D. Faure, Plant sphingolipids: Their importance in cellular organization and adaption, Biochim. Biophys. Acta. 1861 (2016) 1329–1335. https://doi.org/10.1016/j.bbalip.2016.04.003.

[23] M.Y. Wang, Y. Yang, X.Y. Zhou, S.S. Wang, S.X. Duan, X.B. Li, The chemical constituents from *Urtica fissa* leaves, J. Asian Nat. Prod. Res. 20 (2018) 709–718. https://doi.org/10.1080/10286020.2017.1383397.

[24] H. Hussain, A.T. Nyongha, E. Dongo, A. Badshah, I.R. Green, W. Zhang, Melicimides A and B: Two new ceramides from stem bark of *Melicia excelsa*, Rec. Nat. Prod. 7 (2013) 141–146.

[25] J.L. Lü, J.A. Duan, Y.P. Tang, Y.L. Ge, Two new ceramides from the radix of *Angelica sinensis*, J. Chem. Res. (2008) 658–661.

[26] L.A. Tapondjou, A.-C. Mitaine-offer, M. Sautour, Sphingolipids and other constituents from *Cordia platythyrsa*, Biochem. Syst. Ecol. 33 (2005) 1293–1297. https://doi.org/10.1016/j.bse.2005.07.005.

[27] W.Y. Lin, M.H. Yen, C.M. Teng, I.L. Tsai, I.S. Chen, Cerebrosides from the rhizomes of *Gynura japonica*, J. Chinese Chem. Soc. 51 (2004) 1429–1434. https://doi.org/10.1002/jccs.200400211.

[28] C.R. Lee, J.H. Lee, M. Park, K.S. Park, I.K. Bae, Y.B. Kim, S.H. Lee, Biology of *Acinetobacter baumannii*: Pathogenesis, Antibiotic Resistance Mechanisms, and Prospective Treatment Options, Front Cell Infect Microbiol. 7 (2017). https://doi.org/doi: 10.3389/fcimb.2017.00055.

[29] V.G.C. Abreu, J.A. Takahashi, L.P. Duarte, D. Piló-Veloso, P.A.S. Junior, R.O. Alves, A.J. Romanha, A.F.C. Alcântara, Evaluation of the bactericidal and trypanocidal activities of triterpenes isolated from the leaves, stems, and flowers of *Lychnophora pinaster*, Brazilian J. Pharmacogn. 21 (2011) 615–621. https://doi.org/10.1590/S0102-695X2011005000095.

[30] A. Mouts, E. Vattulainen, T. Matsufuji, On the importance of the C(1) -OH and C(3) -OH functional groups of the long-chain base of ceramide for interlipid interaction and lateral segregation into ceramide-rich domains, Langmuir. 34 (2018) 15864–15870. https://doi.org/10.1021/acs.langmuir.8b03237.

[31] J. Liu, W. Yong, Y. Deng, N.R. Kallenbach, M. Lu, Atomic structure of a tryptophan-zipper pentamer, PNAS. 101 (2004) 16156–16161. https://doi.org/10.1073/pnas.0405319101.

[32] K.M. Lamb, M.N. Lombardo, J. Alverson, N.D. Priestley, D.L. Wright, A.C. Anderson, Crystal structures of *Klebsiella pneumoniae* dihydrofolate reductase bound to propargyl-linked antifolates reveal features for potency and selectivity, Antimicrob. Agents Chemother. 58 (2014) 7484–7491. https://doi.org/10.1128/AAC.03555-14.

[33] G. Jepkorir, J.C. Rodríguez, H. Rui, W. Im, S. Lovell, K.P. Battaile, A.Y. Alontaga, E.T. Yukl, P. Moënne-Loccoz, M. Rivera, Structural, NMR spectroscopic, and computational investigation of hemin loading in the hemophore hasap from *Pseudomonas aeruginosa*, J. Am. Chem. Soc. 132 (2010) 9857–9872. https://doi.org/10.1021/ja103498z.

[34] S.P. Bhamidimarri, M. Zahn, J.D. Prajapati, C. Schleberger, S. Söderholm, J. Hoover, J. West, U. Kleinekathöfer, D. Bumann, M. Winterhalter, B. van den

Berg, A Multidisciplinary Approach toward Identification of Antibiotic Scaffolds for *Acinetobacter baumannii*, Structure. 27 (2019) 268–280. https://doi.org/10.1016/j.str.2018.10.021.

[35] R. Fährrolfes, S. Bietz, F. Flachsenberg, A. Meyder, E. Nittinger, T. Otto, A. Volkamer, M. Rarey, ProteinsPlus: a web portal for structure analysis of macromolecules, Nucleic Acids Res. 45 (2017) 337–343. https://doi.org/https://doi.org/10.1093/nar/gkx333.

[36] A.C. Cauz, G.P. Carretero, G.K. V. Saraiva, P. Park, Gueiros-Filho, L. Mortara, I. Cuccovia, M. Brocchi, F.J. Gueiros-Filho, Violacein Targets the Cytoplasmic Membrane of Bacteria, ACS Infect. Dis. 5 (2019) 539–549. https://doi.org/10.1021/acsinfecdis.8b00245.

[37] L.R. Montes, M.B. Ruiz-Argüello, F.M. Goñi, A. Alonso, Membrane restructuring via ceramide results in enhanced solute efflux, J. Biol. Chem. 277 (2002) 11788–11794. https://doi.org/10.1074/jbc.M111568200.

[38] S. Barui, S. Saha, V. Yakati, A. Chaudhuri, Systemic Codelivery of a Homoserine Derived Ceramide Analogue and Curcumin to Tumor Vasculature Inhibits Mouse Tumor Growth, Mol Pharm. 13 (2016) 404–19. https://doi.org/10.1021/acs.molpharmaceut.5b00644.

[39] T. Chipiti, M.A. Ibrahim, M. Singh, M.S. Islam, In vitro α-amylase and α-glucosidase Inhibitory and Cytotoxic Activities of Extracts from *Cissus cornifolia* Planch Parts., Pharmacogn. Mag. 13 (2017) S329–S333. https://doi.org/10.4103/pm.pm_223_16.

[40] I. Artetxe, B. Ugarte-Uribe, D. Gil, M. Valle, A. Alonso, A.J. García-Sáez, F.M. Goñi, A.J. García-Sáez, F.M. Goñi, Does Ceramide Form Channels? The Ceramide-Induced Membrane Permeabilization Mechanism, Biophys J. 113 (2017) 860–868. doi: 10.1016/j.bpj.2017.06.071.

[41] M.B. Ruiz-Argüello, G. Basáñez, F.M. Goñi, A. Alonso, Different effects of enzyme-generated ceramides and diacylglycerols in phospholipid membrane fusion and leakage, J. Biol. Chem. 271 (1996) 26616–26621. https://doi.org/10.1074/jbc.271.43.26616.